Impact of a Localized Source of Subglacial Discharge on the Heat Flux and Submarine Melting of a Tidewater Glacier: A Laboratory Study

CLAUDIA CENEDESE

Physical Oceanography Department, Woods Hole Oceanographic Institution, Woods Hole, Massachusetts

V. MARCO GATTO

Department of Hydraulic Engineering, Delft University of Technology, Delft, Netherlands

(Manuscript received 24 May 2016, in final form 21 August 2016)

ABSTRACT

Idealized laboratory experiments have been conducted in a two-layer stratified fluid to investigate the leading-order dynamics that control submarine melting and meltwater export near a vertical ice–ocean interface as a function of subglacial discharge. In summer, the discharge of surface runoff at the base of a glacier (subglacial discharge) generates strong buoyant plumes that rise along the glacier front entraining ambient water along the way. The entrainment enhances the heat transport toward the glacier front and hence the submarine melt rate increases with the subglacial discharge rate. In the laboratory, the effect of subglacial discharge is simulated by introducing freshwater at freezing temperature from a point source at the base of an ice block representing the glacier. The circulation pattern observed both with and without subglacial discharge resembles those observed in previous observational and numerical studies. Buoyant plumes rise vertically until they find either their neutrally buoyant level or the free surface. Hence, the meltwater can deposit within the interior of the water column and not entirely at the free surface, as confirmed by field observations. The heat budget in the tank, calculated following a new framework, gives estimates of submarine melt rate that increase with the subglacial discharge and are in agreement with the directly measured submarine melting. This laboratory study provides the first direct measurements of submarine melt rates for different subglacial discharges, and the results are consistent with the predictions of previous theoretical and numerical studies.

1. Introduction

Glacial fjords are thought to play an important role in the recent rapid mass loss of the Greenland Ice Sheet (GrIS). Half of the mass loss is linked to the acceleration and retreat of many outlet glaciers (Nick et al. 2009; Vieli and Nick 2011; Howat et al. 2007) and a plausible trigger is the increased submarine melting of glaciers terminating in fjords (Murray et al. 2010; Joughin et al. 2012; Straneo et al. 2013). This hypothesis is consistent with the atmospheric and ocean warming observed around Greenland since the mid-1990s (Holland et al. 2008; Våge et al. 2011; Straneo et al. 2013). Furthermore, fjord processes are responsible for the transformation of the freshwater discharged from Greenland before it is released into the large-scale ocean (Bamber et al. 2012). At present, GrIS mass loss accounts for one quarter of global sea level rise (Shepherd et al. 2012; Church et al. 2011), roughly twice the contribution of the Antarctic Ice Sheet. Knowledge of the fjords' dynamics is thus fundamental to understanding ice sheet variability and its impact on climate (Straneo and Cenedese 2015). The dynamics occurring near the ice, in particular those related to the influence of subglacial discharge on submarine melting, are still poorly understood.

Observations from several fjords suggest that submarine melting and the associated export of meltwaters are affected both by the fjord stratification (Straneo et al. 2011; Mortensen et al. 2011, 2013) and subglacial discharge (Motyka et al. 2013). These findings motivated recent model studies focusing on the role of stratification and subglacial discharge on submarine melt distribution and magnitudes (Jenkins 2011; Xu et al. 2012, 2013;

Corresponding author address: Claudia Cenedese, Physical Oceanography Department, Woods Hole Oceanographic Institution, 360 Woods Hole Road, Woods Hole, MA 02543.
E-mail: ccenedese@whoi.edu

DOI: 10.1175/JPO-D-16-0123.1

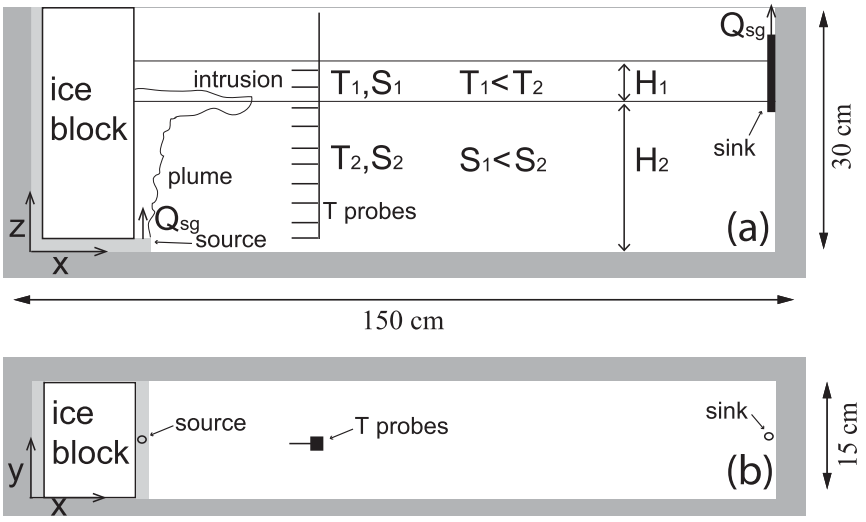

FIG. 1. Laboratory experimental apparatus: (a) side view and (b) top view. Light gray indicates the L-shaped plastic container that was used to store the plastic tube delivering the subglacial discharge Q_{sg} below the ice block. The same volume flux Q_{sg} was withdrawn on the right side of the tank to keep the volume in the tank constant. Not to scale. Adapted from Cenedese and Gatto (2016).

Sciascia et al. 2013, 2014; Motyka et al. 2011, 2013; Kimura et al. 2014; Slater et al. 2015; Carroll et al. 2015). These modeling results, however, are sensitive to the parameterizations of unresolved and poorly understood processes, that is, ice–ocean boundary layer dynamics and melting of the ice front, and caution should be used when making quantitative interpretation of the modeled submarine melting (Straneo and Cenedese 2015).

The current paper presents the first laboratory experiments investigating the influence of a single localized source of subglacial discharge on the submarine melting of a vertical ice face and on the heat flux toward the glacier. The two-layer stratification in the laboratory tank is similar to that found in Sermilik Fjord, where Helheim Glacier terminates, and the subglacial volume flux Q_{sg} was varied. The laboratory results suggest an increase in submarine melting with subglacial discharge. Furthermore, the framework introduced by Jackson and Straneo (2016) provides good estimates of the submarine melt rates and aids in understanding the importance of the different components controlling the heat flux toward the glacier, which ultimately controls the submarine melt rate.

2. Experimental apparatus

The description of the experimental apparatus is similar to that of Cenedese and Gatto (2016). The laboratory experiments were conducted in a rectangular tank, $150 \times 15 \times 30\,\text{cm}^3$ (Fig. 1), that was insulated using triple-paned glass filled with argon. The tank was located in a climate-controlled "cold room" with an approximate constant temperature during each experiment, which varied between $T_{air} = 2.8°\text{C}$ and 3.4°C for the different experiments. In the tank, a two-layer stratification was obtained by adding a bottom layer of depth $H_2' = 20.5\,\text{cm}$ of warmer ($T_2 \approx 3°\text{C}$), saltier ($S_2 \approx 34\,\text{g kg}^{-1}$) water. After this bottom layer came to rest, a cooler ($T_1 \approx 0.5°\text{C}$), fresher ($S_1 \approx 32\,\text{g kg}^{-1}$) second layer of depth $H_1' = 5\,\text{cm}$ was added from a reservoir through a float. The choices of the ratio of the depths of the two layers and their temperatures and salinities were made to match those observed in winter in Sermilik Fjord (Straneo et al. 2010). After residual motions in the two-layer system came to a halt, the experiment started. Consistent with the approach taken in previous experiments (Sciascia et al. 2014; Cenedese and Gatto 2016), the effect of Earth's rotation was ignored. This choice is justified because, in general, in Greenland along-fjord variations tend to dominate over across-fjord variations, consistent with the fact that many fjords are too narrow for the circulation to be significantly influenced by Earth's rotation (e.g., Straneo et al. 2010; Johnson et al. 2011; Sutherland et al. 2014).

A degassed and dyed (blue) ice block ($L_i = 10\,\text{cm}$, $W_i = 15\,\text{cm}$, $H_i = 30\,\text{cm}$) was positioned on the left side of the tank (Fig. 1) to represent a glacier with a vertical face. At the beginning of the experiment the temperature of the ice was $T_i \approx -21°\text{C}$, it increased to a value $T_i \approx -3.5°\text{C}$ during the first 30 min, and then it reached a constant value $T_i \approx -1.6°\text{C}$ after approximately 1 h. The experiment started with the immersion of the ice block on the left side of the tank (Fig. 1), which was done

extremely slowly in order to reduce the motion in the tank and any mixing between the two layers. After the ice block was secured in place, both the subglacial discharge and the sink pumps were started. The immersion of the ice block in the tank caused the total water depth to increase to $H_T = 27$ cm, while the bottom- and top-layer depths increased to $H_2 = 21.7$ cm and $H_1 = 5.3$ cm, respectively. An ''L-shaped'' plastic container was located below the ice block (light gray in Fig. 1) and contained the plastic tube delivering the subglacial discharge to the source located near the bottom edge of the ice block. The source had a diameter $d = 0.22$ cm, was pointed vertically upward, and was positioned halfway across the width of the tank. The ice block distance from the bottom and the left wall of the tank was 2.7 cm. Freshwater dyed red and at the freezing temperature of 0°C was used to simulate the subglacial discharge and the flow rate took the values $Q_{sg} = 0.6$, 1.1, 2.3, and 3.4 $cm^3 s^{-1}$. For the lowest flow rates, the buoyant plume generated by the source of subglacial discharge became fully turbulent within 2 cm from the source, while for the largest flow rates it was fully turbulent much closer to the source. The Reynolds number of the flow at the source $\mathrm{Re} = 4Q_{sg}/(\pi d\nu)$ ($\nu = 0.018\,cm^2 s^{-1}$; the kinematic viscosity of water at 0°C) varied between 193 and 1093 for the range of flow rates listed above.

An oceanic subglacial discharge is expected to have a source that is oriented at an angle with the horizontal but not necessarily vertical. Hence, a subglacial discharge plume in the ocean will initially have both horizontal and vertical momentum components. However, a jet is attracted to a nearby surface due to the Coanda effect (Wille and Fernholz 1965), and numerical simulations suggest that for realistic subglacial discharge flow rates, the subglacial discharge plume loses the horizontal momentum and attaches to the vertical ice front close to the source (Kimura et al. 2014). In the laboratory, the choice of a vertical source of subglacial discharge is therefore suitable for investigating subglacial discharge plumes along a vertical ice front.

On the far side of the tank, opposite the ice block, a sink pipe was connected to a pump to maintain the water volume constant (Fig. 1). The sink was located either near the free surface or near the interface to be at the same level as the intrusion generated by the detachment of the buoyant plume from the ice face (see section 3), and the withdraw flow rate was identical to the subglacial discharge flow rate Q_{sg}. While the total water volume in the tank was constant during an experiment, the temperature and salinity of the two layers on the far side of the tank were not kept constant because the waters of the two layers could not be replenished without further adding to the complexity of the experimental procedure. Hence, the limitation of this experimental set up is that the tank slowly filled up with glacially modified water (see section 3), and all the experiments ended when it reached a depth of 5 cm above the bottom of the tank. Each experiment lasted 25–133 min, and the time was inversely proportional to Q_{sg}, while the experiment with $Q_{sg} = 0\,cm^3 s^{-1}$ lasted 5 h.

The ice block was weighed at the beginning and end of each experiment with a precision of ±5 grams, and the submarine meltwater volume flux is directly measured as

$$Q_{MW} = \frac{M_s - M_e}{\rho_f \Delta t}, \tag{1}$$

where M_s and M_e are the weights of the ice block at the start and end of the experiment, respectively; ρ_f is the freshwater density; and Δt is the duration of the experiment that is known with an error of ±1 min. Ten HOBO Pro v2 temperature dataloggers were mounted at different depths, approximately equally spaced in the vertical, at 25 cm from the ice front (Fig. 1). Measurements were taken every 30 s. Two measures of the horizontal velocity were obtained by dropping potassium permanganate crystals near the center of the tank approximately when the glacially modified water intrusion (see section 3) reached the end of the tank and when it reached half of the total water depth. Digital movies of the purple streaks left behind by the crystals were taken from the side of the tank, and their analysis gives two measures of the horizontal velocity at two different times at the depth corresponding to the location of the temperature probes. A total of four experiments with different values of Q_{sg} were conducted, and one experiment with no subglacial discharge.

3. Subglacial discharge plume

The subglacial discharge generates a buoyant plume that ascends vertically along the ice face, entraining both ambient waters and submarine meltwaters, and forming what we will call in the remainder of the paper ''glacially modified waters.'' Although submarine melting is present, the primary buoyancy source is provided by the subglacial discharge that generates a vigorous plume (Fig. 2b), and the dynamics observed near the ice edge are in agreement with the ''convection-driven melting'' regime (Motyka et al. 2003; Jenkins 2011). In the absence of subglacial discharge, a weaker buoyant plume (Fig. 2a) is generated solely by the submarine melting, and it rises vertically, entraining ambient waters. The observed behavior in this experiment is indicative of the ''melt-driven convection'' regime (Jenkins 2011).

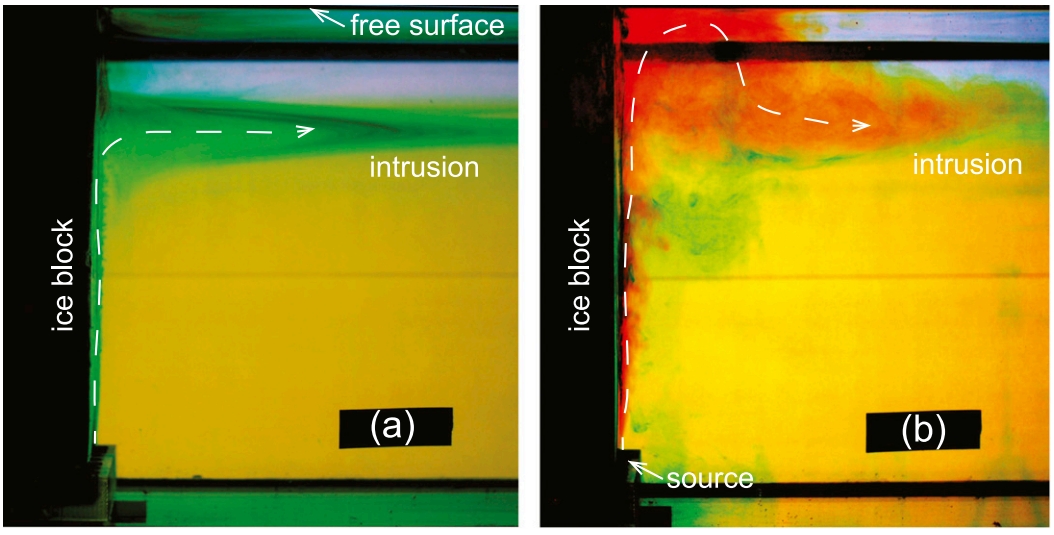

FIG. 2. Side view of the ice block face on the left and the buoyant plume for Q_{sg} = (a) 0 and (b) 2.3 $cm^3 s^{-1}$. (a) In the absence of subglacial discharge, the buoyant plume is weaker and forms an intrusion at the interface. The plume is green (blue) in the lower (upper) layer because the meltwater from the blue ice block mixes with the ambient yellow (clear) fluid. The top blue plume is very weak due to the top layer's low temperature. (b) When a high subglacial discharge is present (dyed red), the plume overshoots its neutrally buoyant level, reaches the free surface, and then readjusts downward to form an intrusion between the two layers.

The buoyant plume detaches from the vertical ice front and forms an intrusion at the interface between the two layers if its density at the interface depth is larger than the top-layer density (Fig. 2a). At the beginning of the experiment, for the parameters investigated in this study, the main intrusion always occurs at the interface between the two layers. However, for low subglacial discharges ($Q_{sg} \leq 1.1\,cm^3 s^{-1}$), a small fraction of the plume is able to rise to the free surface. In these experiments, two intrusions, one at the interface and one at the free surface, are observed to move glacially modified waters away from the ice face. A possible explanation for the generation of the free-surface intrusion is that the plume density is not homogeneous, especially when the plume is less vigorous, and the portion of the plume closer to the ice face maintains a density lower than the top-layer density, allowing the fluid to reach the free surface and form a surface intrusion moving into the fjord. In the laboratory, we can use color to distinguish between the buoyant plume created by the combined subglacial discharge and the ice block melting (mainly red from the subglacial discharge; Fig. 2b) and the plume created above the interface solely from the ice block melting into the upper clear layer, which instead is blue due to the ice block being dyed blue. The blue plume is only observed in the absence of subglacial discharge ($Q_{sg} = 0\,cm^3 s^{-1}$). For low subglacial discharges ($0 < Q_{sg} \leq 1.1\,cm^3 s^{-1}$), as discussed above, a small fraction of the plume forced by the subglacial discharge does rise all the way to the free surface to form a surface intrusion. Furthermore, for high subglacial discharges ($Q_{sg} \geq 1.1\,cm^3 s^{-1}$), the plume forced by the subglacial discharge is observed to have enough vertical momentum to overshoot its neutrally buoyant level, reach the free surface, and then readjust downward to form an intrusion between the two layers (Fig. 2b).

In summary, the experimental results suggest that the glacially modified water can intrude at depth and not only at the free surface, as also previously observed in numerical studies (Sciascia et al. 2013; Xu et al. 2012, 2013) and field studies in Sermilik Fjord (Straneo et al. 2011).

4. Control volume heat budget

Oceanic measurements of heat transport have been used to determine submarine melting of marine-terminating glaciers in Greenland fjords (e.g., Sutherland and Straneo 2012; Rignot et al. 2010; Motyka et al. 2013). A recent study by Jackson and Straneo (2016) addressed the heat, salt, and mass budgets in a fjord and developed a new framework for inferring freshwater fluxes from these budgets. Following their derivation, we obtain the heat budget for the control volume enclosed by the dashed black lines in Fig. 3 that is bounded by the tank bottom, lateral walls, free surface, ice block, and a section X located 25 cm from the ice front, where the temperature measurements have been conducted. As illustrated

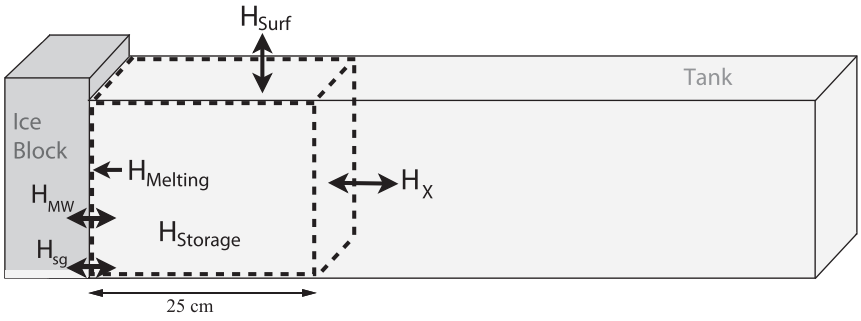

FIG. 3. Heat budget schematic for the control volume indicated by the dashed black line. Adapted from Jackson and Straneo (2016).

schematically in Fig. 3, the heat budget is composed of six terms: the heat transport through the cross section $X H_X$, the heat transport from subglacial discharge H_{sg} and submarine melting H_{MW}, the change in heat content of the control volume $H_{Storage}$, the heat flux through the free surface H_{Surf}, and the heat lost to submarine melting $H_{Melting}$. Hence, the heat budget can be written as

$$\underbrace{\rho c_p \int_{A_X} uT\,dA}_{H_X} + \underbrace{\rho c_p Q_{sg} T_{sg}}_{H_{sg}} + \underbrace{\rho c_p Q_{MW} T_{MW}}_{H_{MW}} = \underbrace{\rho c_p \frac{\partial}{\partial t}\int_{V_c} T\,dV}_{H_{Storage}} + \underbrace{\rho L_{adj} Q_{MW}}_{H_{Melting}} + H_{Surf}, \tag{2}$$

where A_X is the cross section X area; $H_{Melting}$ and H_{Surf} are positive if the control volume loses heat; u and T are the velocity (positive toward the ice block) and temperature measurements, respectively, at the cross section X; ρ is the density of water; c_p is the heat capacity of water; L_{adj} is an adjusted latent heat to take into account both the latent heat to melt ice and the heat required to raise the ice temperature to the melting temperature [see Jackson and Straneo (2016) for details]; Q_{sg} and Q_{MW} are the subglacial discharge and submarine meltwater volume fluxes, respectively; and T_{sg} and T_{MW} are their respective temperatures. Assuming that H_{Surf} is small, that the control volume is unchanged (i.e., either the ice volume lost to melting is small compared to the control volume or the ice front location is fixed), that the velocity at the cross section X is the same as in the center of the tank where the measurements were taken, and decomposing the velocity and temperature signal into a barotropic and a baroclinic part, that is, $u = u_0 + u'$ and $T = T_0 + T'$, (2) can be rearranged to obtain

$$\underbrace{\rho c_p \int_{A_X} u'T'\,dA}_{H'} + \underbrace{\rho c_p Q_{sg}(T_{sg} - T_0) + \rho c_p Q_{MW}(T_{MW} - T_0)}_{H_0 + H_{sg} + H_{MW}} = \underbrace{\rho c_p \frac{\partial}{\partial t}\int_{V_c} T\,dV}_{H_{Storage}} + \underbrace{\rho L_{adj} Q_{MW}}_{H_{Melting}}, \tag{3}$$

where $H_X = H_0 + H'$ and H_0 (H') is the heat transport associated with the barotropic (baroclinic) flow. Furthermore, we assumed that to conserve mass in the control volume the barotropic velocity through the cross section X must balance the freshwater inputs, that is, $-u_0 A_X = Q_{sg} + Q_{MW}$. We note that in the laboratory $Q_{MW} \ll Q_{sg}$ for values of $Q_{sg} > 0\,\mathrm{cm^3\,s^{-1}}$ (Fig. 5a). The velocity and temperature decompositions are obtained using the following expressions:

$$u_0 = \frac{1}{A_X}\int_{A_X} u\,dA, \quad u' = u - u_0, \quad \text{and} \tag{4}$$

$$T_0 = \frac{1}{A_X}\int_{A_X} T\,dA, \quad T' = T - T_0. \tag{5}$$

The first term on the lhs of (3) is the heat flux advected by the baroclinic flow; the second term is the sum of the heat flux advected by the barotropic flow and the freshwater inputs due to subglacial discharge and submarine melting. These two terms are balanced by the change in heat content of the control volume, that is, the first term on the rhs, and the heat lost to submarine melting, that is, the second term on the rhs. The full rigorous derivations of (2) and (3) can be found in

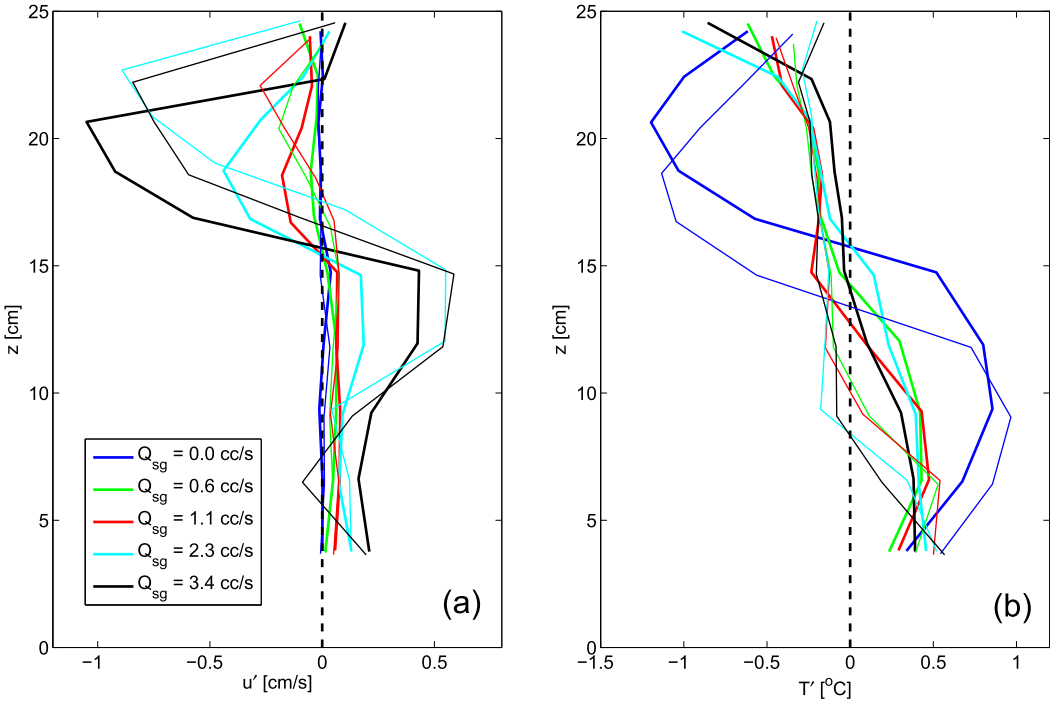

FIG. 4. Vertical profiles of baroclinic (a) velocity u' and (b) temperature T'. The interface between the two layers is located at approximately $z = 20$ cm. Thicker (thin) lines represent an earlier (later) in time profile. Positive velocities are toward the ice block.

Jackson and Straneo (2016). We note that in our derivation of (3) we did not need the salt budget equation as in Jackson and Straneo (2016) because we know Q_{sg} a priori, and we can use the conservation of the mass equation to estimate u_0 given the fact that, as in the ocean (Jackson and Straneo 2016), this quantity cannot be measured reliably in the laboratory, as explained in detail in section 5.

5. Fjord circulation and submarine melting

The circulation in the tank is characterized by an intrusion of glacially modified waters that move away from the ice front along the interface between the two layers (Fig. 2) and with a velocity that increases with increasing Q_{sg} (Fig. 4a). The entrainment in the subglacial discharge plume induces a velocity in the bottom layer toward the ice front and that again increases with increasing Q_{sg}. This circulation transports relatively warmer waters toward the ice front and moves relatively cold waters away from it (Fig. 4b). Conservation of mass suggests that the barotropic component of the velocity field u_0 is one to two orders of magnitude smaller than the baroclinic component u' (Fig. 4a). In agreement with this result, the laboratory measurements indicate that $|u_0| \ll \max(|u'|)$. However, the uncertainty in the velocity measurement makes the laboratory estimate of u_0 [(4)] indistinguishable from zero.

The control volume heat budget [(3)] can be used to obtain estimates of the heat lost to submarine melting and therefore the submarine meltwater volume flux Q_{MW}. This estimate can be compared with the direct measure of ice melting [(1)], as shown in Fig. 5a. The agreement between the measured and estimated submarine meltwater volume flux is good, suggesting that the assumptions made in section 4 are reasonable. The various terms in (3) are plotted in Fig. 5b, and they all increase in magnitude with increasing subglacial discharge with the exception of $H_{Melting}$ that for the two largest values of Q_{sg} has approximately the same value. For small values of Q_{sg} the term $H_{Storage}$ is small, and the heat provided to submarine melting is given by the heat transport associated with the baroclinic flow. However, for large values of Q_{sg} all the terms in (3) need to be considered for an accurate estimate of $H_{Melting}$.

Previous studies (Jenkins 2011; Xu et al. 2012; Sciascia et al. 2013) suggest that in the convection-driven melting regime, that is, $Q_{sg} \gg Q_{MW}$, submarine melt rate should increase with the subglacial discharge with a power-law exponent of 1/3. However, the melt

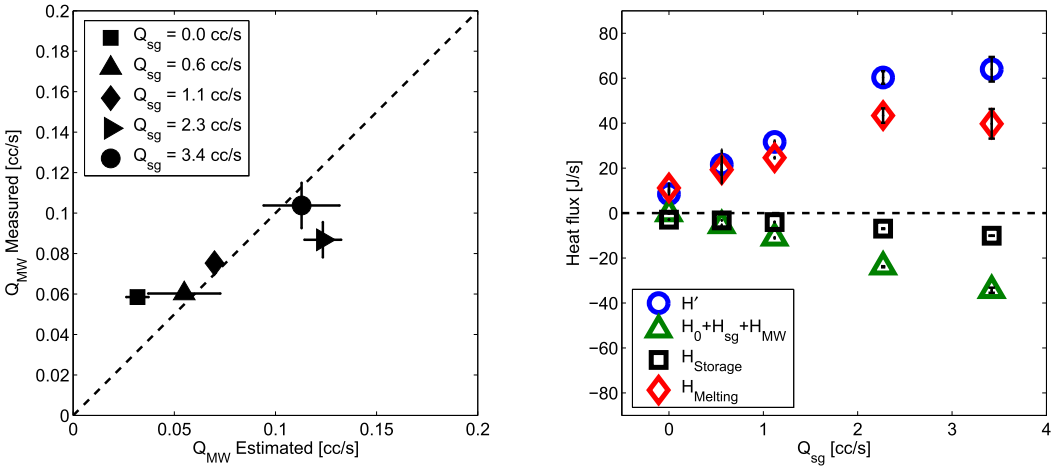

FIG. 5. (a) Submarine meltwater volume flux directly measured by weighing the ice block, that is, (1), and estimated using the control volume heat budget, that is, (3), for different subglacial discharges. Dashed line represents the 1:1 slope. (b) Magnitude of the different terms in (3) for different subglacial discharges. Symbols are the averages between the two estimates obtained with the two different measurements of temperature and velocity at two different times. Error bars are given by the values of the two estimates, for the estimated Q_{MW}, and calculated from the uncertainties in the measurement of Δt and the ice block mass, for the measured Q_{MW}.

rate measured in the laboratory experiments includes both the melt rate due to the plume forced by subglacial discharge, that is, convection-driven melting, and the melting occurring in the region outside the plume due to melt-driven convection. Using plume theory as in Cenedese and Gatto (2016), one can estimate the ratio of the area of the ice block face covered by the plume to the remaining area. This ratio varies with subglacial discharge and ranges from 0.33 to 0.85 for Q_{sg} varying from 0.6 to 3.4 $cm^3 s^{-1}$. Hence, albeit the directly measured submarine melt rate increases with subglacial discharge (Fig. 6), the 1/3 scaling is not necessarily expected to hold for the measured melting that also includes the melting in the region outside the plume.

6. Conclusions

Subglacial discharge at the base of a glacier generates a buoyant plume that rises vertically until it finds its level of neutral buoyancy or the free surface. In this laboratory study submarine melting is directly measured and does not depend on parameterizations of unresolved processes. Submarine melting is observed to increase with increasing subglacial discharge, consistent with previous theoretical and numerical results that parameterize the ice–ocean boundary and melting processes (Jenkins 2011; Xu et al. 2012; Sciascia et al. 2013). The novel framework introduced by Jackson and Straneo (2016) for a complete and rigorous heat, salt, and mass budget in a fjord was employed with the laboratory data and the estimate of submarine melting was in good agreement with the directly measured submarine melting.

The importance of subglacial discharge on both the circulation in the tank and the submarine melting suggests that the discharge details in a marine terminating glacier are of primary importance for a correct prediction of these variables. Furthermore, understanding of the small-scale processes

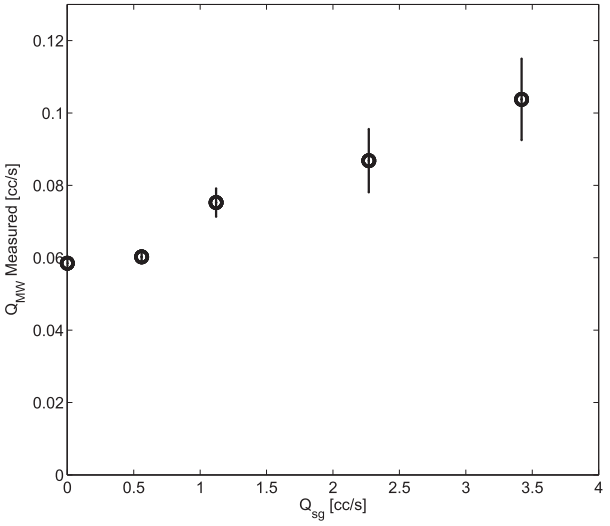

FIG. 6. The directly measured submarine meltwater volume flux increases with increasing subglacial discharges. Error bars are as in Fig. 5.

influencing plume dynamics and submarine melting is fundamental for their correct parameterization in numerical models.

Acknowledgments. The authors thank Jason Hyatt and Rebecca Jackson for helpful comments on the manuscript and Anders Jensen for the able assistance in the laboratory. Support to C. C. was given by the NSF project OCE-1130008 and OCE-1434041. M. G. received support from the "Gori" Fellowship.

REFERENCES

Bamber, J., M. van den Broeke, J. Ettema, J. Lenaerts, and E. Rignot, 2012: Recent large increases in freshwater fluxes from Greenland into the North Atlantic. *Geophys. Res. Lett.*, **39**, L19501, doi:10.1029/2012GL052552.

Carroll, D., D. A. Sutherland, E. L. Shroyer, J. D. Nash, G. A. Catania, and L. A. Stearns, 2015: Modeling turbulent subglacial meltwater plumes: Implications for fjord-scale buoyancy-driven circulation. *J. Phys. Oceanogr.*, **45**, 2169–2185, doi:10.1175/JPO-D-15-0033.1.

Cenedese, C., and V. M. Gatto, 2016: Impact of two plumes' interaction on submarine melting of tidewater glaciers: A laboratory study. *J. Phys. Oceanogr.*, **46**, 361–367, doi:10.1175/JPO-D-15-0171.1.

Church, J. A., and Coauthors, 2011: Revisiting the earth's sea-level and energy budgets from 1961 to 2008. *Geophys. Res. Lett.*, **38**, L18601, doi:10.1029/2011GL048794.

Holland, D. M., R. H. Thomas, B. De Young, M. H. Ribergaard, and B. Lyberth, 2008: Acceleration of Jakobshavn Isbrae triggered by warm subsurface ocean waters. *Nat. Geosci.*, **1**, 659–664, doi:10.1038/ngeo316.

Howat, I. M., I. Joughin, and T. A. Scambos, 2007: Rapid changes in ice discharge from Greenland outlet glaciers. *Science*, **315**, 1559–1561, doi:10.1126/science.1138478.

Jackson, R. H., and F. Straneo, 2016: Heat, salt, and freshwater budgets for a glacial fjord in Greenland. *J. Phys. Oceanogr.*, **46**, 2735–2768, doi:10.1175/JPO-D-15-0134.1.

Jenkins, A., 2011: Convection-driven melting near the grounding lines of ice shelves and tidewater glaciers. *J. Phys. Oceanogr.*, **41**, 2279–2294, doi:10.1175/JPO-D-11-03.1.

Johnson, H., A. Münchow, K. Falkner, and H. Melling, 2011: Ocean circulation and properties in Petermann Fjord, Greenland. *J. Geophys. Res.*, **116**, C01003, doi:10.1029/2010JC006519.

Joughin, I., R. B. Alley, and D. M. Holland, 2012: Ice-sheet response to oceanic forcing. *Science*, **338**, 1172–1176, doi:10.1126/science.1226481.

Kimura, S., P. Holland, A. Jenkins, and M. Piggott, 2014: The effect of meltwater plumes on the melting of a vertical glacier face. *J. Phys. Oceanogr.*, **44**, 3099–3117, doi:10.1175/JPO-D-13-0219.1.

Mortensen, J., K. Lennert, J. Bendtsen, and S. Rysgaard, 2011: Heat sources for glacial melt in a sub-Arctic fjord (Godthåbsfjord) in contact with the Greenland Ice Sheet. *J. Geophys. Res.*, **116**, C01013, doi:10.1029/2010JC006528.

——, J. Bendtsen, R. J. Motyka, K. Lennert, M. Truffer, M. Fahnestock, and S. Rysgaard, 2013: On the seasonal freshwater stratification in the proximity of fast-flowing tidewater outlet glaciers in a sub-Arctic sill fjord. *J. Geophys. Res. Oceans*, **118**, 1382–1395, doi:10.1002/jgrc.20134.

Motyka, R. J., L. Hunter, K. A. Echelmeyer, and C. Connor, 2003: Submarine melting at the terminus of a temperate tidewater glacier, LeConte Glacier, Alaska, USA. *Ann. Glaciol.*, **36**, 57–65, doi:10.3189/172756403781816374.

——, M. Truffer, M. Fahnestock, J. Mortensen, S. Rysgaard, and I. Howat, 2011: Submarine melting of the 1985 Jakobshavn Isbræ floating tongue and the triggering of the current retreat. *J. Geophys. Res.*, **116**, F01007, doi:10.1029/2009JF001632.

——, W. P. Dryer, J. Amundson, M. Truffer, and M. Fahnestock, 2013: Rapid submarine melting driven by subglacial discharge, Leconte Glacier, Alaska. *Geophys. Res. Lett.*, **40**, 5153–5158, doi:10.1002/grl.51011.

Murray, T., and Coauthors, 2010: Ocean regulation hypothesis for glacier dynamics in southeast Greenland and implications for ice sheet mass changes. *J. Geophys. Res.*, **115**, F03026, doi:10.1029/2009JF001522.

Nick, F. M., A. Vieli, I. M. Howat, and I. Joughin, 2009: Large-scale changes in Greenland outlet glacier dynamics triggered at the terminus. *Nat. Geosci.*, **2**, 110–114, doi:10.1038/ngeo394.

Rignot, E., M. Koppes, and I. Velicogna, 2010: Rapid submarine melting of the calving faces of west Greenland glaciers. *Nat. Geosci.*, **3**, 187–191, doi:10.1038/ngeo765.

Sciascia, R., F. Straneo, C. Cenedese, and P. Heimbach, 2013: Seasonal variability of submarine melt rate and circulation in an east Greenland fjord. *J. Geophys. Res. Oceans*, **118**, 2492–2506, doi:10.1002/jgrc.20142.

——, C. Cenedese, D. Nicoli, P. Heimbach, and F. Straneo, 2014: Impact of periodic intermediary flows on submarine melting of a Greenland glacier. *J. Geophys. Res. Oceans*, **119**, 7078–7098, doi:10.1002/2014JC009953.

Shepherd, A., and Coauthors, 2012: A reconciled estimate of ice-sheet mass balance. *Science*, **338**, 1183–1189, doi:10.1126/science.1228102.

Slater, D. A., P. W. Nienow, T. R. Cowton, D. N. Goldberg, and A. J. Sole, 2015: Effect of near-terminus subglacial hydrology on tidewater glacier submarine melt rates. *Geophys. Res. Lett.*, **42**, 2861–2868, doi:10.1002/2014GL062494.

Straneo, F., and C. Cenedese, 2015: Dynamics of Greenland's glacial fjords and their role in climate. *Annu. Rev. Mar. Sci.*, **7**, 89–112, doi:10.1146/annurev-marine-010213-135133.

——, G. Hamilton, D. Sutherland, L. Stearns, F. Davidson, M. Hammill, G. Stenson, and A. Rosing-Asvid, 2010: Rapid circulation of warm subtropical waters in a major glacial fjord in east Greenland. *Nat. Geosci.*, **3**, 182–186, doi:10.1038/ngeo764.

——, R. Curry, D. Sutherland, G. Hamilton, C. Cenedese, K. Vage, and L. Stearns, 2011: Impact of fjord dynamics and glacial runoff on the circulation near Helheim Glacier. *Nat. Geosci.*, **4**, 322–327, doi:10.1038/ngeo1109.

——, and Coauthors, 2013: Challenges to understand the dynamic response of Greenland's marine terminating glaciers to oceanic and atmospheric forcing. *Bull. Amer. Meteor. Soc.*, **94**, 1131–1144, doi:10.1175/BAMS-D-12-00100.1.

Sutherland, D. A., and F. Straneo, 2012: Estimating ocean heat transports and submarine melt rates in Sermilik Fjord, Greenland, using lowered acoustic Doppler current profiler (LADCP) velocity profiles. *Ann. Glaciol.*, **53**, 50–58, doi:10.3189/2012AoG60A050.

——, ——, and R. S. Pickart, 2014: Characteristics and dynamics of two major Greenland glacial fjords. *J. Geophys. Res. Oceans*, **119**, 3767–3791, doi:10.1002/2013JC009786.

Våge, K., and Coauthors, 2011: The Irminger Gyre: Circulation, convection, and interannual variability. *Deep-Sea Res. I*, **58**, 590–614, doi:10.1016/j.dsr.2011.03.001.

Vieli, A., and F. Nick, 2011: Understanding and modelling rapid dynamic changes of tidewater outlet glaciers: Issues and implications. *Surv. Geophys.*, **32**, 437–458, doi:10.1007/s10712-011-9132-4.

Wille, R., and H. Fernholz, 1965: Report on the first European mechanics colloquium, on the Coanda effect. *J. Fluid Mech.*, **23**, 801–819, doi:10.1017/S0022112065001702.

Xu, Y., E. Rignot, D. Menemenlis, and M. Koppes, 2012: Numerical experiments on subaqueous melting of Greenland tidewater glaciers in response to ocean warming and enhanced subglacial runoff. *Ann. Glaciol.*, **53**, 229–234, doi:10.3189/2012AoG60A139.

——, ——, I. Fenty, D. Menemenlis, and M. M. Flexas, 2013: Subaqueous melting of store glacier, west Greenland from three-dimensional, high-resolution numerical modeling and ocean observations. *Geophys. Res. Lett.*, **40**, 4648–4653, doi:10.1002/grl.50825.